Homologous series of LC acrylic monomers based on phenyl benzoate core group: synthesis and characterisation

P. Romero-Hasler, D. Arismendi, P. Richter & E. A. Soto-Bustamante

Taylor & Francis
Taylor & Francis Group

Check for updates

Homologous series of LC acrylic monomers based on phenyl benzoate core group: synthesis and characterisation

P. Romero-Hasler [iD][a], D. Arismendi[b], P. Richter [iD][b] and E. A. Soto-Bustamante [iD][a]

[a]Department of Organic and Physical Chemistry, Faculty of Chemical and Pharmaceutical Sciences, University of Chile, Santiago, Chile; [b]Department of Inorganic and Analytical Chemistry, Faculty of Chemical and Pharmaceutical Sciences, University of Chile, Santiago, Chile

ABSTRACT
The synthesis and phase characterisation of a homologous series of monomers of acrylic phenyl benzoates has been carried out. The characterisation comprises polarised optical microscopy, differential scanning calorimetry and powder x-ray diffractometry. All monomers are mesogenic, exhibiting either nematic and/or smectic phase. Shorter monomers are nematogenic while longer monomers show a more smectogenic character. Most of the monomers show monotropic phases.
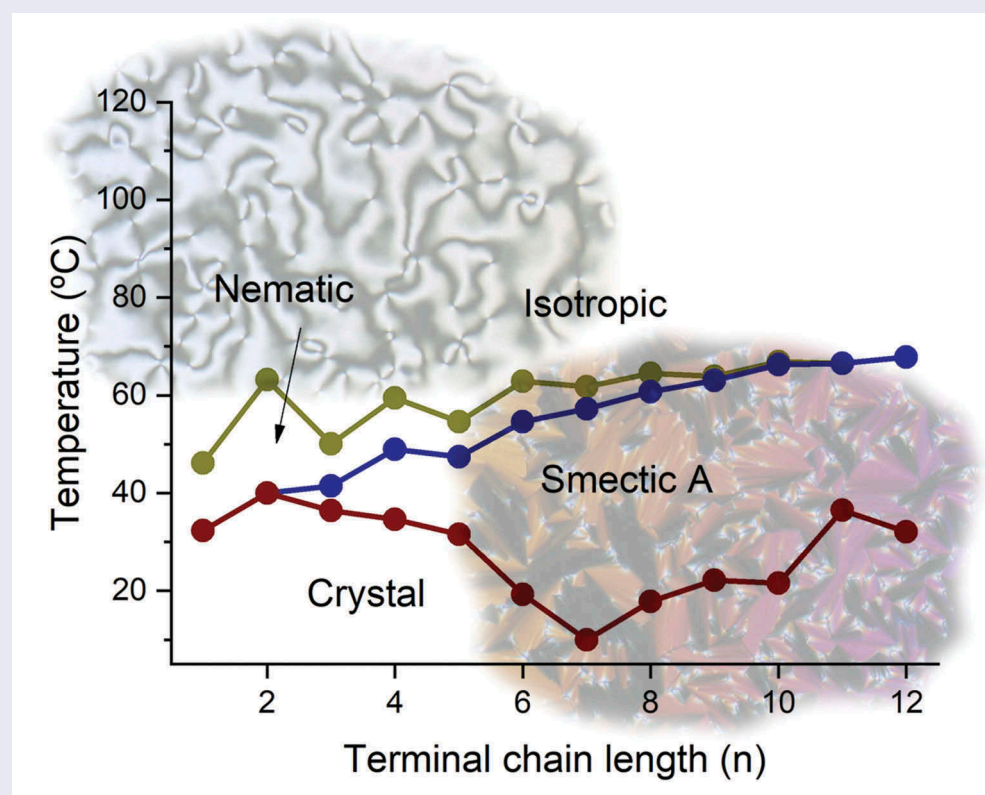
1. Introduction

In this article, we will study a new electrically induced polymerisation process, carried out in the molten state. This occurs by the application of a DC field on a molten mesogenic monomer (liquid crystalline or isotropic) without added electrolytes or solvents as regular electrochemical polymerisation systems [1]. This produces the respective side-chain liquid crystalline polymer. The monomers are confined inside glass cells with their facing surfaces covered by deposited electrodes. Additionally, these surfaces may have an alignment-inducing layer on them. The last is also mandatory to obtain a highly aligned polymer which follows the buffing direction.

Supplemental data for this article can be accessed here.

In order to study this polymerisation process, we previously synthesised two families of acrylic monomers with an azobenzene group as aromatic core A6An and A6OAn [2]. However, they did not yield good results in the polymerisation system due to the inhibitor character of the 4,4′-azobenzene group on radical polymerisation [3]. Despite the difficulty of its polymerisation, the azo monomer A6A12 was studied in mixtures with a nematic and a ferroelectric liquid crystal host to observe its effects in a polymer-stabilised system [4]. Polymer was formed on the cell substrates and acted as a second alignment layer.

As a next step in this research, we decide to synthesise acrylic monomers possessing phenyl benzoate core, which does not hinder the polymerisation as has been previously observed in an M11E12 methacrylic monomer [1] synthesised in our group.

The nomenclature used throughout this paper is based on previously synthesised compounds [2]. For this family of 4-[6-(acryloyloxy)hexyloxy]-4′-(alkyloxy) phenyl benzoates, we use the A6E*n* acronym. A stands for a polymerisable acrylate group, linked through a six-methylene unit as spacer (6) to the phenyl benzoate core

(E) via an ether link in *para* position. The phenyl benzoate core (E) has also a terminal alkyloxy chain with *n* carbon atoms in *para* position of the phenyl moiety. The series synthesised has variable terminal chain from 1 to 12 carbon units. Figure 1 shows both the synthetic pathway and the general structure of the monomers A6E*n*.

Four members of these phenyl benzoate monomers (A6E1, A6E2, A6E4 and A6E6) have been previously synthesised by Portugal et al. [5], Horváth et al. [6], Shindo et al. [7] and Yoshida et al. [8]. These results are summarised in Table 2. We observed a similar behaviour which confirms to some extent what has been reported. As far as we know, the rest of the monomers have not been reported thoroughly: A6E3, A6E5, A6E7, A6E8, A6E9, A6E10, A6E11 and A6E12.

2. Experimental

2.1. Materials and methods

Hydroquinone (HQ), alkyl bromides (n-Br) and *N,N'*-dicyclohexylcarbodiimide were obtained from Merck
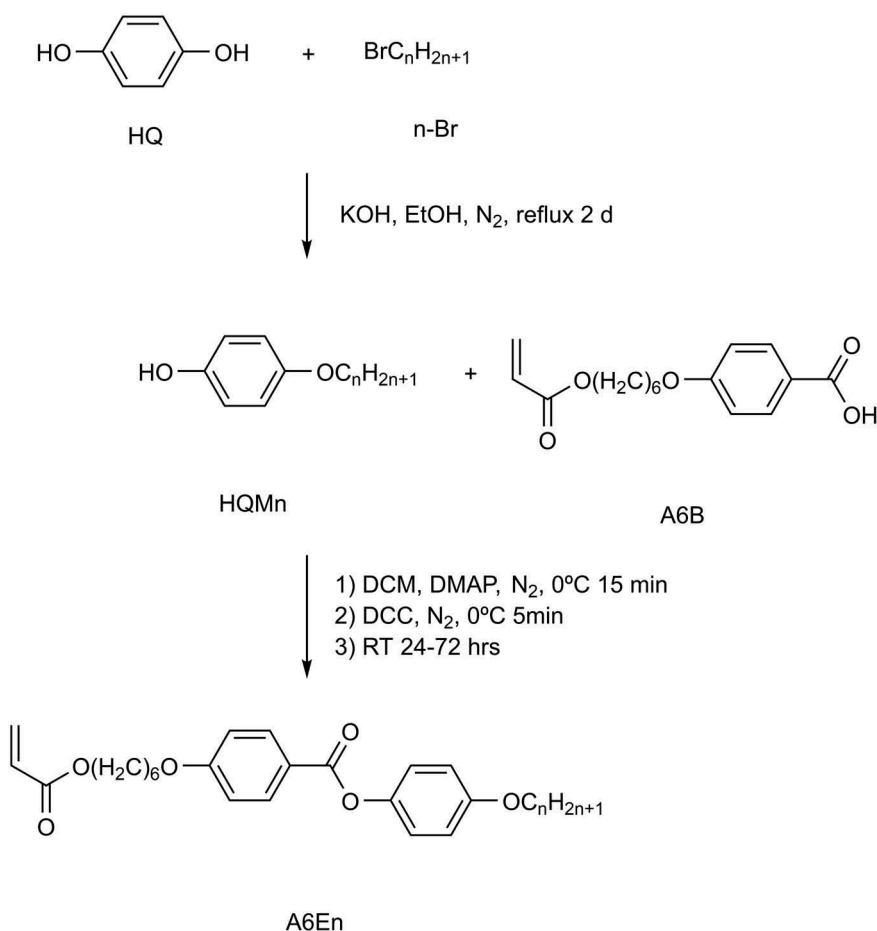

Figure 1. Synthetic pathway for the synthesis of A6E*n* monomers.

(Germany). 4-Dimethylamino pyridine (DMAP) was obtained from Sigma-Aldrich (USA). 4-(6-(Acryloyloxy)hexyloxy) benzoic (A6B) acid was obtained from Synthon chemicals (Germany). All other reagents and solvents are Pro Analysis grade, obtained from Merck and used as received.

2.2. Synthesis

The synthesis of the 12 monomers was carried out using a convergent synthetic pathway, summarised in Figure 1.

2.2.1. Synthesis of 4-dodecyloxyphenol (HQM12)
The n-alkylokyphenols (HQMn) were synthesised through a Williamson etherification [9] as follows.

In a dried 250-ml round-bottom flask, 10 g (5 eq) of HQ and 13.5 g (1 eq) of 12-bromodecane are weighted, dissolved in 100 ml of ethanol and refluxed under nitrogen atmosphere under stirring over 2–6 h. A solution of potassium hydroxide, 3.05 g (1 eq) dissolved in 10 ml of ethanol was added dropwise and the reaction mixture allowed to reflux for 24 h under nitrogen atmosphere. The reaction mixture was neutralised with 2N HCl, vacuum-dried, extracted with DCM, dried with Na_2SO_4 and purified through flash chromatography using silica gel 60 as stationary phase and 6:1 hexane/ethyl acetate as mobile phase. After this, the product was recrystallised in petroleum ether (40–60°C bp). The white product yields 10.1 g, 67%.

[1] H-NMR, δ ppm, $CDCl_3$: 8.13 (d, $^3J_{AB}$ = 3.5 Hz, 4H, H_B–Ar); 4.44 (s, 1H, HO–Ar); 3.89 (t, ^3J = 6.59 Hz, 2H, αCH_2–O–); 1.73 (p, ^3J = 6.59 Hz, 2H, βCH_2–O–); 1.42 (p, ^3J = 6.60 Hz, 2H, γCH_2–O–); 1.37–1.18 (m, 16H, –CH_2–); 0,87 (t, ^3J = 6.65 Hz, 3H, CH_3–).

2.2.2. Synthesis of 4'-dodecyloxyphenyl 4-(6-(acryloyloxy)hexyloxy))benzoate (A6E12)
The synthesis of the final monomer A6E12 was obtained by a Steglich esterification [10] of the A6B acid and the formerly synthesised 4-alkyloxyhydroquinones (HQM12).

In a previously flame-dried 300-ml Erlenmeyer flask, 9.5 g (1.2 eq) of A6B, 7.59 g (1 eq) of 4-dodecyloxyphenol (HQM12) and 0.33 g (0.1 eq) of DMAP are weighted. The flask is sealed with a rubber septum, and 100 ml of anhydrous dichloromethane (DCM) is injected. The flask is cooled in an ice bath and purged with nitrogen gas. After 10 min of cooling, 5.62 g (1 eq) of dicyclohexylcarbodiimide dissolved in 50 ml of anhydrous DCM is slowly added with a syringe over 1 min. The mixture is further kept in the ice bath during 5 min under a nitrogen purge and then left to react sealed for 24–48 h at room temperature.

The reaction mixture is vacuum-dried and pre-purified through flash chromatography using silica gel 60 as stationary phase and DCM as mobile phase, collecting the first fraction. This fraction shows three spots on thin layer chromatography (TLC) with 3:1 hexane/ethyl acetate as mobile phase and is recrystallised one to three times in ethanol or acetone/water mixture. The silvery white product yields 10.85 g, 78%.

Mass spectromery (electrospay ionisation) – MS (ESI): Calculated mass (M-Na$^+$): 575.3343, Found mass (M-Na$^+$): 575.3448.

[1] H-NMR, δ ppm, $CDCl_3$: 8.13 (d, $^3J_{AB}$ = 8.89 Hz, 2H, H_B–Ar); 7.09 (d, $^3J_{CD}$ = 9.02 Hz, 2H, H_C–Ar); 6.96 (d, $^3J_{AB}$ = 8.89 Hz, 2H, H_A–Ar); 6.91 (d, $^3J_{CD}$ = 9.08 Hz, 2H, H_D–Ar); 6.41 (dd, $^3J_{trans}$ = 17.31 Hz, ^2J = 1.51 Hz, 1H, transCH_2=CH–); 6.13 (dd, $^3J_{trans}$ = 17.31 Hz, $^3J_{cis}$ = 10.38 Hz, 1H, CH_2=CH–); 5.82 (dd, $^3J_{cis}$ = 10.38 Hz, ^2J = 1.50 Hz, 1H, cisCH_2=CH–); 4.18 (t, ^3J = 6.63 Hz, 2H, αCH_2–O–); 4.05 (t, ^3J = 6.39 Hz, 2H, αCH_2–O–); 3.95 (t, ^3J = 6.54 Hz, 2H, αCH_2–O–); 1.91–1.65 (m, 6H, βCH_2–O–); 1.57–1.39 (m, 6H, γCH_2–O–); 1.38–1.17 (m, 16H, –CH_2–); 0.88 (t, ^3J = 6.61 Hz, 3H, CH_3–).

2.3. Characterisation

The ^{1}H-NMR spectra were obtained from a Bruker AVANCE DRX 300 spectrometer operating at 300.13 MHz. Measurements were carried out at a probe temperature of 300 K, using $CDCl_3$ containing TMS as internal standard.

Identification of monomers was performed by MS using an AxION 2 TOF-MS system equipped with a dual-probe ultraspray electrospray ionisation source and controlled by TOF MS Driver Software (PerkinElmer, USA).

Synthesised compounds dissolved in acetone containing formic acid (0.1% v/v) were injected separately by direct infusion into the mass spectrometer at a rate of 50 μL/min. The working conditions were as follows: capillary voltage of 6000 V, capillary exit of −125 V, gas flow rate of 10 L/min, gas temperature of 300°C and nebuliser pressure in both probes of 80 psi. MS accurate mass spectra were recorded across a range of 100–1200 m/z. The uncertainty associated with the mass measurement was set at 20 ppm for all compounds. All the compounds were ionised in positive mode. To improve the sensitivity of the analysis, the acquisition function was in trap mode, setting the parameters 'IG Exit Low' and 'Trap/Pulse Delay' at 25 and 45 μs, respectively.

Table 1. Phase transitions and enthalpies associated with A6E*n* family.

A6E*n*		Phase transitions by heating T (°C) – ΔH (kJ/mol)	Phase transitions by cooling T (°C) – ΔH (kJ/mol)
1	Temp	Cr – 58.8 – I	I – 46.2 – N – 27.7 – Cr
	ΔH	Cr – 32.2 – I	I – −0.9 – N – −28.0 – Cr
2	Temp	Cr – 105.8 – I	I – 63.2 – N – 40.3 – Cr
	ΔH	Cr – 62.1 – I	I – −0.9 – N – −40.3 – Cr
3	Temp	Cr – 71.5 – I	I – 50.3[b] – N – 41.6[b] – SmA – 37.8 – Cr
	ΔH	Cr – 42.4 – I	I – −0.6[b] – N – −0.6b – SmA – −30.6 – Cr
4	Temp	Cr – 62.9 – I	I – 59.6[b] – N – 49.2[b] – SmA – 45.2[b] – Cr
	ΔH	Cr – 45.7 – I	I – −0.9[b] – N – −0.6[b] – SmA – −35.9[b] – Cr
5	Temp	Cr – 57.1 – I	I – 54.6 – N – 47.4 – SmA – 31.5 – Cr
	ΔH	Cr – 45.0 – I	I – −0.7 – N – −1.5 – SmA – −29.2 – Cr
6	Temp	Cr – 57.9 – N – 62.8[c] – I	I – 62.3 – N – 54.1 – SmA – 19.2 – Cr
	ΔH	Cr – 47.4 – N – 0.7[c] – I	I – −1.0 – N – −1.2 – SmA – −20.8 – Cr
7	Temp	Cr – 61.9 – N – 61.9[c] – I	I – 61.0 – N – 56.5 – SmA – 19.0 – Cr
	ΔH	Cr – 43.0 – N – n.d. – I	I – −0.8 – N – −2.5 – SmA – −20.7 – Cr
8	Temp	Cr – 61.5 – N – 61.6[c] – I	I – 64.2 – N – 60.9 – SmA – 24.3 – Cr
	ΔH	Cr – 39.2 – N – 0.8[c] – I	I – −1.1 – N – −2.3 – SmA – −24.9 – Cr
9	Temp	Cr – 65.8 – I	I – 63.9[a] – N – 63.1[a] – SmA – 22.1 – Cr
	ΔH	Cr – 42.9 – I	I – −1.0 – N – −2.3 – SmA – −27.6 – Cr
10	Temp	Cr – 67.5 – I	I – 66.9[a] – N – 66.3[a] – SmA – 21.6 – Cr
	ΔH	Cr – 51.3 – I	I – −0.5 – N – −3.3 – SmA – −30.1 – Cr
11	Temp	Cr – 69.5 – I	I – 66.6 – SmA – 36.5 – Cr
	ΔH	Cr – 46.8 – I	I – −4.5 – SmA – −35.1 – Cr
12	Temp	Cr – 72.1 – I	I – 67.8 – SmA – 32.1 – Cr
	ΔH	Cr – 55.3 – I	I – −4.9 – SmA – −30.2 – Cr

Scan rate 10°C/min, [a]Scan rate 2°C/min, [b]Scan rate 30°C/min, [c]Scan rate 0.5°C/min, n.d., not determined.

Table 2. Phase transition temperature comparisons.

	Portugal et al. [5]	Horváth et al. [6]	Shindo et al. [7]	Yoshida et al. [8]	This work
A6E1	Cr 53 I	Cr 48 LC 54 I		Cr 52 LC 57, 8 I	Cr 58.8 I
		I 54 LC 48 Cr			I 46, 2N 27, 7 Cr
A6E2	Cr 56N 63 I		I 46 Cr	Cr 93, 9 LC 102 I	Cr 105.8 I
					I 63, 2N 40, 3 Cr
A6E4		Cr 54 LC 58 I			Cr 62.9 I
					I 59, 6N 49, 2 SmA 45,2 Cr
A6E6			I 62N 55S 26 Cr	Cr 52, 8 LC 57, 8 I	Cr 57.91N 62.83 I
					I 62, 3N 54,1 SmA 19, 2 Cr

The thermal behaviour of the compounds has been determined via a TA Q20 differential scanning calorimetry (DSC) using sealed aluminium pans (TA T-Zero pans) under a nitrogen purge (50 ml/min) and a heating and cooling rate of 10°C/min unless otherwise noted. The DSC was calibrated using indium (156.6°C) and a ramp rate of 10°C/min. As control, we used three different temperature standards: benzophenone (ME18870) m.p. 47.9 ± 0.2°C, benzoic acid (ME18555) m.p. 122.3 ± 0.2°C and caffeine (ME18872) m.p. 236.0 ± 0.3°C.

A polarised microscope (Leica, DLMP), equipped with a heating stage (Instec, HCS302/STC200), was used for temperature-dependent investigations of liquid crystal (LC) textures between glass substrates, which was coupled with a Canon 750D camera for obtaining photomicrographs. The samples were supported between Elvamide 8023R-coated glass plates for planar alignment microphotographs and on Instec cells with 20 μm cell gap and homeotropic-alignment-inducing layers (SB100A200uT180) for conoscopic observations.

Variable temperature powder X-ray measurements were carried out using a Cu lamp diffractometer. The wavelength used for calculation is considered as CuKa$_1$ at 1.540562 Å. These values were corrected using silver behenate (AgBh) as small-angle standard [11] and silicon (NIST SRM 640b) as wide-angle standard. The samples were studied by cooling using a focusing horizontal two-circle X-ray diffractometer (STOE, STADI-P) with a linear position-sensitive detector [12,13]. The samples were contained in 1.0-mm glass capillaries (Lindemann) and held in a modified Instec HCS402 stage in which the temperature was stabilised within the range 30–100°C during the measurements.

The smectic layer distance (d) was obtained from the small-angle 001 reflex according to Bragg's law. The theoretical molecular length (L) for all compounds was obtained with Gaussian 2009 [14], using DFT with hybrid B3LYP 6-21G basis set, measuring the distance between the furthest axial hydrogens.
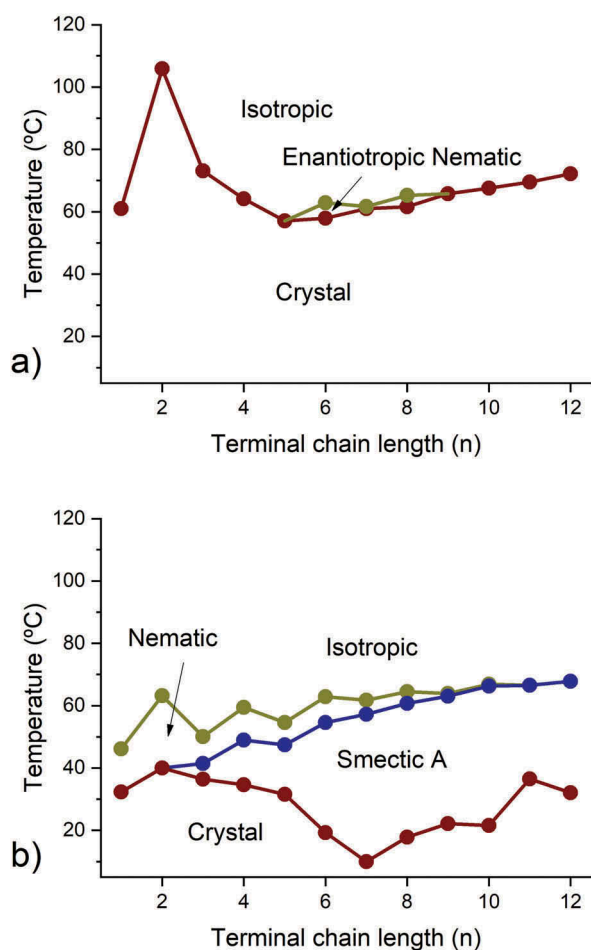
Figure 2. (Colour online) Phase diagrams for the synthesised A6E*n* family: (a) heating; (b) cooling.

3. Results

3.1. Synthesis of compounds

The synthesised compounds were confirmed by attenuated total reflection–Fourier-transform spectroscopy (ATR-FTIR), ^{1}H-NMR spectroscopy and ESI-MS.

3.2. Attenuated total reflection–Fourier-transform infrared spectroscopy

The obtained ATR-FTIR data are consistent with the expected molecular structure. Supplementary Figure 1 shows the spectrum for A6E12 with its more important bands highlighted. At 3078 cm^{-1} the sp^{2}C–H stretching modes of the vinylic and aromatic moieties appear; at 2939 and 2866 cm^{-1}, the sp^3 CH stretching modes of the aliphatic chains; at 1733 and 1720, the vinylic and aromatic C=O stretching, respectively; at 1637 cm^{-1}, the C=C stretching for the vinylic group; at 1606 and 1510 cm^{-1}, the sp^2 C=C stretching of the aromatic core; at 1412 cm^{-1}, C=C–H in-plane bending for vinylic

group; between 1300 and 1100 cm^{-1}, several stretching bands of the C–O bonds on the esters; at 987 cm^{-1}, the =CH2 wagging of the acrylic moiety and at 813 cm^{-1} the acrylic C=C–H out of plane bending.

3.3. Proton nuclear magnetic resonance

Proton nuclear magnetic resonance analysis agrees with the structure of the synthesised molecules. Supplementary Table 1 summarises the chemical shifts obtained for the whole series. We observe the two *para*-substituted benzenic ring protons as duplets around 8.2 and 6.8 ppm as duplets. The acrylic protons are observed between 6.5 and 5.7 ppm, each of them as double duplets. The proton in the methylenedioxy moiety appears between 4.3 and 3.8 ppm as triplets, the next methylene between 2.0 and 1.4 ppm as quintuplets and the subsequent methylenes are observed as a multiplet between 1.4 and 1.1 ppm. Finally, the terminal methyl group appears as a triplet, except for A6E1, where it is directly bonded to the oxygen as a methoxy and therefore just a singlet appears at 3.83 ppm. For the rest of A6E*n*, it appears as a triplet, and it shifts to higher field with increasing chain length, stabilising around 0.89 ppm for A6E8 and onwards.

3.4. MS analysis

Supplementary Table 2 shows the results found by direct infusion of the compound solutions in the TOF-MS equipment. The success of the synthesis of acrylate monomers was confirmed through high-resolution MS and the comparison with theoretical data. In all cases, the expected ionised molecules were found with errors in the detection between −3 and −20 ppm, which indicates the high accuracy of the data obtained.

In ESI sources, it is common to find molecules in the form of adducts with alkaline metals such as sodium (Na) and potassium (K), which can arise from the reagents used during the synthesis or as part of the impurities found through the methodology [15,16]. The three ions found by each monomer (Supplementary Table 2) can be assigned to the formation of [M + Na]$^+$, [M + K]$^+$ and [2M + Na]$^+$ adducts, respectively.

3.5. Polarised light microscopy and DSC

All the monomers obtained show mesomorphic behaviour. The phase diagrams by heating and cooling are shown in Figure 2 and were obtained using DSC data. Besides A6E6–A6E8, the observed mesophases are

monotropic. Monotropic phases are metastable phases that can only be seen by cooling and require the super-cooling of the more stable phase, in this case, the crystal-line phase [17]. While monotropic phases are not thermodynamically stable, they can be obtained kineti-cally due to the slow nucleation and growth of crystal phase.

Monomers with short tails (A6E1 and A6E2) show a monotropic nematogenic behaviour. For A6E3 and A6E4, we see a monotropic smectic A (smA) phase, which is only observed at fast cooling rates. At slower cooling rates (5°C/min), only crystallisation from the nematic is seen. In this case, the appearance of the mesophase is kinetically controlled. From A6E5 up to A6E12, we see a more stable monotropic smA phase. Beginning from A6E1, the nematic temperature range decreases while the smectic range increases up to A6E10; for A6E11 and A6E12, only a smA phase was observed. The presence of a nematic phase for shorter tail calamitic molecules with a decreasing range and a smectic behaviour for longer tails with an increasing range is widely known and has been described for other similar series [18–20].

Nematic phases show a schlieren texture on Elvamide-treated glass substrates, while the smectic phase shows smooth focal conic texture (see Figure 3(a,b)). In cells with homeotropic alignment, the smectic phase is dark for all monomers under crossed polarisers. We see a symmetric cross (isogyres) under conoscopic illumina-tion with a Bertrand lens (see Figure 3(c)). Then, the smectic phase obtained is orthogonal (smA phase).

Table 1 shows the phase transition temperatures and corresponding enthalpies obtained by DSC, at a heating and cooling rate of 10°C/min. For samples with unstable phases, we used faster rates, while for compounds with narrow phases, we used slower rates to enhance the resolution of the phase transition temperatures and enthalpies.

In the case of A6E3 and A6E4, to observe the SmA phase coexisting with the crystal phase, the cooling rate was 30°C/min. To detect the enantiotropic nematic phase, we use 0.5°C/min as heating rate for A6E6, A6E7 and A6E8. To evaluate the phase transition tem-perature and enthalpy of the narrow nematic phase in A6E8, A6E9 and A6E10, we use a 2°C/min cooling rate.

Regarding the obtained enthalpies, the measured N-I enthalpies range between 0.5 and 1.2 kcal/mol. For the phase transition from isotropic state to nematic state, a clear even–odd effect was observed in the series related to the alkoxy substitution length. Considering the for-mer publication of Marčelja [21], this is a well-known effect seen in almost all studies of homologous series of liquid crystals (LCs). It was described from an entropic

point of view of the chain ordering in liquid crystals. The increasing length of alkyl chain by the addition of further carbon atoms increases the anisotropy of the molecule helping the ordering and disordering process. The effect is progressively small, being almost unnotice-able for long end chains.

For the nematic to smA phase transition, a mono-tonic decrease in the enthalpy is observed while the alkyl chain is shortest. Either smectic or nematic liquid crys-talline phase to crystalline state as expected is the largest
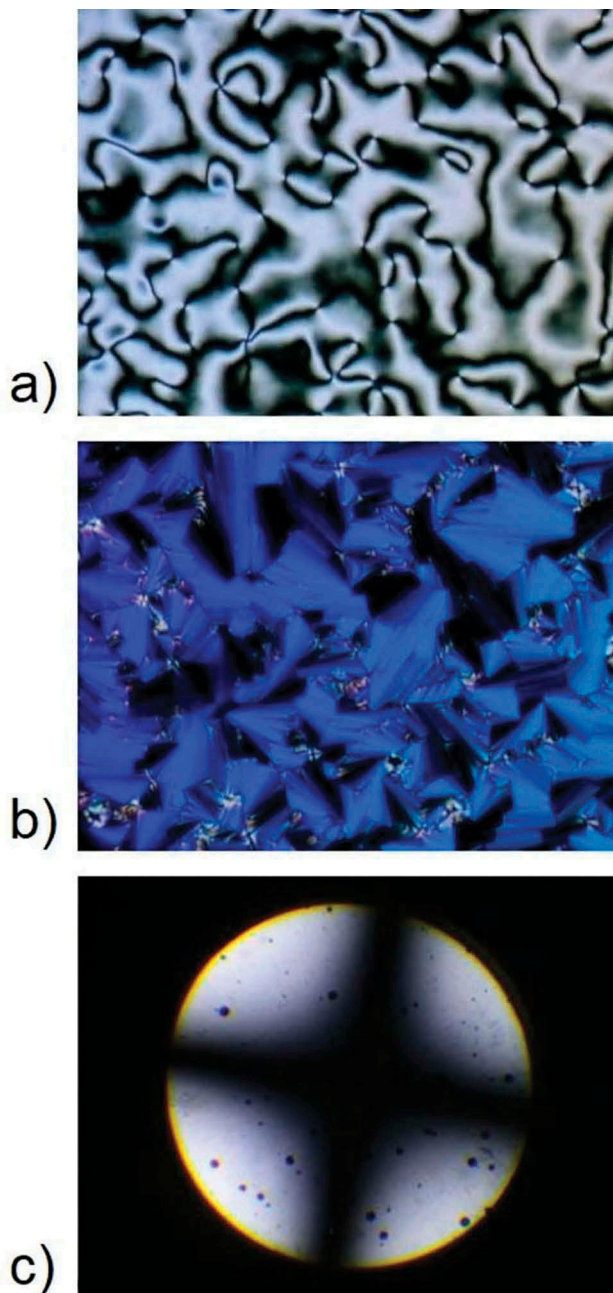

Figure 3. (Colour online) Microphotographs by cooling with 20× magnification for A6E6: (a) schlieren texture (N, 58°C); (b) focal conic texture (smA, 40°C); (c) conoscopy of the smA phase.

energy needed for phase transition, exhibiting 20–40 kcal/mol. The magnitudes of the observed enthalpies are comparable for the values observed for other series of LC compounds with similar structure [22,23].

The obtained mesomorphic behaviour is similar to the one reported in literature by other authors [5–8]. However, there are significant differences between these data. We will address the results reported for A6E1, A6E2, A6E4 and A6E6 in Table 2.

For A6E1, A6E2, A6E4 and A6E6, the values we obtained are similar to the one reported in literature. Our results show also a monotropic nematic phase except for A6E6, A6E7 and A6E8, where the nematic phase is enantiotropic with a quite narrow temperature range. Interestingly, this behaviour appears for monomers which are symmetric in length, where the terminal alkoxy chain 6, 7 and 8 are comparable in length to the 6-(acryloyloxy)hexyloxy moiety A6. This can be understood by the complementary length of the acrylic spacer and alkyloxy terminal tail length, which shows a better packing in the lamellar phase. Aromatic to aliphatic comparable length increase the mesophase stability. This effect was also reported in previously synthesised azobenzene homologues [2].

For A6E1, we observed only a monotropic nematic phase. Portugal et al. described the synthesis and phase behaviour of liquid crystalline polyacrylates, reporting the synthesis and characterisation of the corresponding LC acrylic monomers. They reported this compound as non-mesogenic, describing only the melting point which agrees with ours. Portugal et al. do not specify if the sample was studied by heating or cooling, neither the rate used. Through their observation, we believe the crystallisation would be at 53°C by cooling. In this case, their sample would not be supercooled enough to observe the metastable nematic at 46°C seen by us (Table 2). For the same compound, Horvath et al. reported a liquid crystalline phase between 54°C and 48°C which is roughly 8°C lower than our observed value. Yoshida et al. reported liquid crystalline phase at 52°C which is enantiotropic. However, their DSC traces show highly endothermic peaks, which agree with crystal-crystal transitions and not a crystal–LC and an LC-I transition.

For A6E2, it behaves similar to A6E1; however, the melting point is higher than the whole series (106°C), expressing also a monotropic nematic phase appearing at 63°C by cooling. Portugal et al. mention the nematic phase; however, they report a melting point of 56°C which is remarkably lower than our observations. We assume their temperature was observed by cooling. Shindo et al. report A6E2 without mesomorphic

behaviour, which would be easily explained if they observed the crystallisation by cooling at higher temperatures than our observed nematic phase, for which the sample must be drastically supercooled. Yoshida et al. report an enantiotropic mesogenic phase at 94°C; however, the peaks observed in their DSC traces agree more with a Cr–Cr transition instead of an LC phase formation.

For A6E4, we observed a monotropic N and a monotropic smA phase in the range 59–49°C and 49–45°C, respectively. Only Horvath reported this monomer, observing one liquid crystalline phase between 58°C and 54°C. In our case, the observed smA phase appears only at fast cooling conditions, since the crystallisation occurs rapidly, and the nematic–smectic transition seems to be concurrent with a nematic–crystal transition. If Horvath et al.'s observations were carried out at low cooling rates, is understandable that they did not observe the smA phase.

Finally, for A6E6, we observed an enantiotropic nematic phase at 62–54°C and a monotropic smA phase at 54–20°C, respectively. The nematic phase is close to the crystal melting and can be easily overlooked at high heating rates. Our observations agree with Shindo et al.; however, they differ again from the observations of Yoshida et al. who reported a liquid crystalline phase between 58°C and 52°C. In this case, once again their DSC traces agree more with Cr-Cr and Cr-I transitions than Cr-LC and LC-I transitions.

Summarising our findings are somehow consistent with previously reported compounds [5–8]. We observe a clear monotropic behaviour which was not explicitly reported, most probably due to the high supercooling required to observe it. The more contradicting findings are with Yoshida et al., who report enantiotropic behaviour for A6E1, A6E2 and A6E6, which seems to be misinterpreted crystal–crystal transitions, since their DSC peaks are too high to be mesophase–isotropic transitions.

3.6. X-ray diffraction investigations

Figure 4 shows representative diffractograms of the observed mesophases. The nematic phase possesses no long-range positional order showing just one diffuse reflex at small angles and a diffuse reflex at wide angle (Figure 4(a)). The one-dimensional detection and the absence of alignment in the capillary does not allow us to unequivocally differentiate it from the isotropic state. The existence of this phase is supported by polarised optical microscopy (POM) (Figure 3). The smectic phases show a pseudo-Bragg peak at low angles due to its lamellar nature (Figure 4(b)), while on the wide-angle region, we see only a diffuse peak. This means that we have only a low-order smectic phase. Table 3
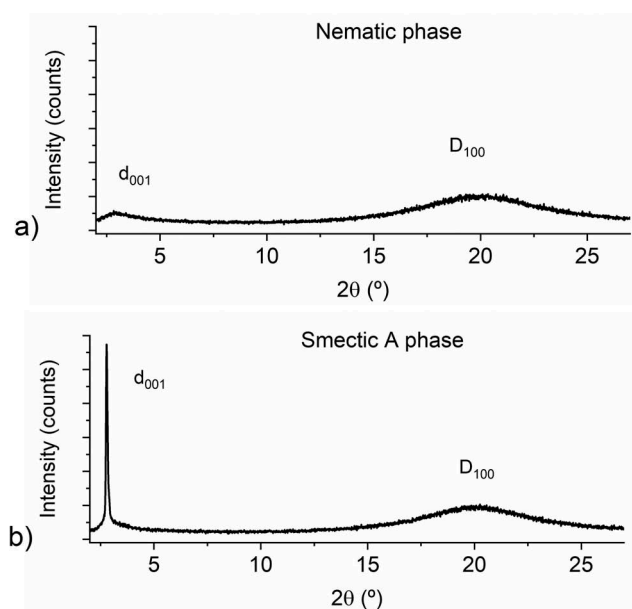
Figure 4. Full x-ray diffraction patterns for A6E6 inside the (a) nematic (60°C) and (b) smectic A phase (50°C).

summarises the theoretical molecular length l_{theo} for each monomer; the observed molecular length dobs at a certain temperature and the observed/theoretical molecular length ratio (d_{obs}/l_{teo}) at several temperatures.

Figure 5 summarises the smA phase interlayer distance vs. temperature for all the monomers studied. In this figure, the nematic isotropic phase transition estimated from POM observations is also included.

The diffraction data obtained correlate well with the POM and DSC studies. The only smectic phase observed was the smA phase, as shown by POM with conoscopic observation. The d-spacings obtained

behave in accordance with an orthogonal lamellar phase, while the diffuse wide-angle reflex agrees with a liquid-like intra-layer order. The layer spacings show a slight decrease when decreasing the temperature, which is consistent with the thermal contraction of the phase when cooled. All monomers show a slight deviation from its theoretical length obtained for the most extended conformation, which may be explained either by a small interdigitation of the terminal aliphatic chains or due to arrangement via the so-called zigzag model [24,25]. In this model, the chains are in part non-collinear with the rigid core; by shortening the molecular length, effect is more pronounced in monomers with longer terminal chains. In our case, the d_{obs}/l_{theo} (see Table 3) corroborates this assumption.

It is noteworthy to mention that we did not observe any thermal polymerisation either by POM, DSC or by powder x-ray diffractometry (PXRD) measurements in the range of days, which makes these monomers fully reliable for further polymerisation studies in liquid crystalline or isotropic melt.

4. Conclusions

The synthesis and characterisation of a homologous family of acrylic phenyl benzoate monomers was carried out.

Their mesomorphic properties were assessed by POM, DSC and PXRD. They show thermotropic liquid crystalline phases with increasing order while increasing the length of terminal alkoxy tail. Shorter members with one and two methylenic groups show only a nematic
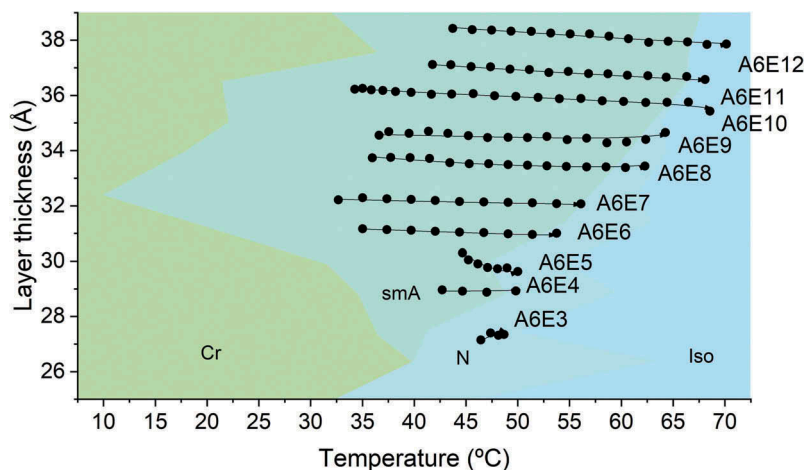

Figure 5. (Colour online) Temperature dependence of the interlayer distance under cooling for the smectic A phase in the A6E*n* (*n* = 3–12) monomer series. The coloured background of nematic and smectic A phases is from POM observations.

Table 3. XRD layer spacing for the A6E*n* family.

Monomer	Temperature (°C)	d_{obs} (Å)	l_{theo} (Å)	d_{obs}/l_{theo}
A6E1	–	–	24.90	−26.30
A6E2	–	–	26.30	–
A6E3	48.7	27.34	27.40	1.00
A6E4	49.8	28.93	28.80	1.00
A6E5	49.4	29.72	29.90	0.99
A6E6	53.7	31.00	31.30	0.99
A6E7	56.0	32.07	32.40	0.99
A6E8	62.3	33.44	33.90	0.99
A6E9	63.3	34.44	35.00	0.98
A6E10	66.5	35.76	36.40	0.98
A6E11	68.1	36.57	37.50	0.98
A6E12	70.1	37.87	38.90	0.97

phase, while longer members (3–10) exhibit nematic and smectic phases. Terminal chains from 11 to 12 carbon atoms show only one smA phase.

The phase stability with temperature behaves as expected. The nematic phase range decreases with longer terminal chains while the smA phase range increases with longer terminal chains.

Only A6E6, A6E7 and A6E8 show enantiotropic nematic phases, all other mesophases being monotropic.

Disclosure Statement

No potential conflict of interest was reported by the authors.

ORCID

P. Romero-Hasler 🆔 http://orcid.org/0000-0002-9211-2514
P. Richter 🆔 http://orcid.org/0000-0002-7978-0657
E. A. Soto-Bustamante 🆔 http://orcid.org/0000-0002-0735-5715

References

[1] Soto-Bustamante E, Trujillo-Rojo V, In situ polymerisation process for obtaining an electro-optical apparatus, said polymer and electro-optical apparatus; and uses there of. US Pat. App. 13/982,522. 2012

[2] Romero-Hasler PR, Fierro-Armijo AEE, Soto-Bustamante EAA, et al. Synthesis and characterisation of two homologous series of LC acrylic monomers based on phenolic and resorcinic azobenzene groups. Liq Cryst. 2016;43:1804–1812.

[3] Szakács S, Jókay L, Földes-Bereznich T, et al. The kinetics of radical polymerization—XXVII. Investigation of the radical reactivity of 3,3'- and 4,4'-disubstituted azobenzenes in the polymerization of vinylacetate. Eur Polym J. 1978;14:181–184.

[4] Kasch N, Dierking I, Turner M, et al. Liquid crystalline textures and polymer morphologies resulting from electropolymerisation in liquid crystal phases. J Mater Chem C. 2015;3:8018–8023.

[5] Portugall M, Ringsdorf H, Zentel R. Synthesis and phase behaviour of liquid crystalline polyacrylates. Die Makromol Chemie. 1982;183:2311–2321.

[6] Horváth J, Nyitrai K, Cser F, et al. Polimerizáció folyadékkristályban, XVII. Á mezogén oldallánc lágy szubsztituensek hatása a mezogén polimerek tulajdonságaira. Magy Kémiai Folyóirat. 1984;90:270–280.

[7] Shindo T, Uryu T. Synthesis and solid-state polymerization of liquid-crystalline acrylic monomers containing chiral epoxy groups. Polym J. 1990;22:336.

[8] Yoshida K, Kakuchi T. UV curable coatings with mesogenic side groups. Prog Org Coatings. 2005;52:165–172.

[9] Naish-Byfield S, Cooksey CJ, Latter AM, et al. In vitro assessment of the structure-activity relationship of tyrosinase-dependent cytotoxicity of a series of substituted phenols. Melanoma Res. 1991;1:273–287.

[10] Wang Z. Steglich catalyst. Comprehensive organic name reactions and reagents. Hoboken, NJ, USA: John Wiley & Sons, Inc.; 2010. p. 2651–2655.

[11] Huang TC, Toraya H, Blanton TN, et al. X-ray powder diffraction analysis of silver behenate, a possible low-angle diffraction standard. J Appl Crystallogr. 1993;26:180–184.

[12] Fan ZX, Haase W. Determination of the translational order parameter in the liquid crystalline smectic A phase using the x-ray diffraction method. J Chem Phys. 1991;95:6066–6074.

[13] Klämke W, Fan ZX, Haase W, et al. An experimental setup for x-ray investigations on higher ordered liquid crystals. Berichte der Bunsengesellschaft für. Phys Chemie. 1989;93:478–482.

[14] Frisch MJ, Trucks GW, Schlegel HB, et al. Gaussian 09, Revision A.01., Gaussian, Inc., Wallingford, CT; 2009.

[15] Kostiainen R, Kauppila TJ. Effect of eluent on the ionization process in liquid chromatography–mass spectrometry. J Chromatogr A. 2009;1216:685–699.

[16] Banerjee S, Mazumdar S. Electrospray ionization mass spectrometry: a technique to access the information beyond the molecular weight of the analyte. Int J Anal Chem. 2012;2012:1–40.

[17] Neubert ME. Characterization of mesophase types and transitions. In: Kumar S, editor. Liquid crystals: experimental study of physical properties and phase transitions. Cambridge, UK: Cambridge University Press; 2001. p. 29–64.

[18] Hird M. Relationship between molecular structure and transition temperatures for calamitic structures. In: Luckhurst GR, Fukuda A, Dunmur D, et al., editors. Physical properties of liquid crystals: nematics. London, UK: Institution of Electrical Engineers; 2001. p. 671.

[19] Neubert ME, Wildman PJ, Zawaski MJ, et al. The effect of carbonyl containing substituents in the terminal chains on mesomorphic properties in aromatic esters and thioesters, 2. Acyloxy groups on the phenolic. End Mol Cryst Liq Cryst. 1987;145:111–157.

[20] Neubert ME, Blair TT, Dixon-Polverine Y, et al. A reassessment of the trends in mesomorphic properties observed in 4,4′-alkylalkoxyphenylbenzoates: molecular crystals and liquid crystals incorporating nonlinear optics. Mol Cryst Liq Cryst Inc Nonlinear Opt. 1990;182(1):269–286.

[21] Marčelja S. Chain ordering in liquid crystals. I. Even-odd effect. J Chem Phys. 1974;60:3599–3604.

[22] Levine AW, Tomeczek KD. Enthalpy of fusion of nematogens. Mol Cryst Liq Cryst. 1977;43:183–187.

[23] Acree WE, Chickos JS. Phase change enthalpies and entropies of liquid crystals. J Phys Chem Ref Data. 2006;35:1051–1330.

[24] Ostrovskii BI X-ray diffraction study of nematic smectic A and C liquid crystals [Internet]. Harwood Academic Publishers; 1989.

[25] Bartolino R, Doucet J, Durand G. Molecular tilt in the smectic C phase: a zigzag model. Ann Phys (Paris). 1978;3:389–395.